Materials Today Nano 30 (2025) 100629

Contents lists available at ScienceDirect

Materials Today Nano

journal homepage: www.sciencedirect.com/journal/materials-today-nano

Reducing friction and wear with alkyl gallate additives in water-based lubricants

Yun Long [a], Jean Michel Martin [a], Frederic Dubreuil [a], Benoit Thiebaut [b], Sophie Loehle [b], Huong T.T. Ta [c], Mauro Ferrario [c,d], M. Clelia Righi [c,**], Maria-Isabel De Barros Bouchet [a,*]

[a] Ecole Centrale de Lyon, Laboratory of Tribology and System Dynamics, CNRS UMR 5513, 36 Avenue Guy de Collongue, 69134, Ecully Cedex, France
[b] TotalEnergies, OneTech Fuels & Lubricants, Research Center Solaize, Solaize, 69360, France
[c] Department of Physics and Astronomy, University of Bologna, Bologna, 40127, Italy
[d] FIM Department, University of Modena and Reggio E, Modena, 41125, Italy

ARTICLE INFO

Keywords:
Eco-friendly gallates
Polyalkylene glycol
Friction modifier
Anti-Wear agent
Machine learning interaction potentials

ABSTRACT

Environmental concerns have made the development of non-flammable, high-specific heat capacity, and high-performance lubricants an urgent priority, driving an increased demand for aqueous-based formulations. A key challenge for their widespread application is achieving low friction across a broad range of speeds. A low-viscosity system composed of polyalkylene glycol (PAG), water, and diethylene glycol offers superlubricity (i.e., friction coefficient $\leq$0.01) at rolling speeds above 150 mm/s; however, significant friction remains at lower rolling or sliding speeds. This limitation can be addressed by introducing eco-friendly and non-toxic gallate molecules. For example, adding 1 % lauryl gallate stabilizes the friction coefficient at approximately 0.04 with no measurable wear. To activate the anti-friction and anti-wear properties of gallates, the molecules must have alkyl chains with eight or more carbon atoms.

Large-scale molecular dynamics simulations have been conducted to explore the key mechanisms by which gallate molecules achieve such superior lubricity. This is made possible through innovative machine learning techniques that enable simulations with Density Functional Theory (DFT) accuracy, allowing the modeling of large systems over extended timescales. Simulations reveal that the superior lubricity of gallates results from the strong anchoring of molecular patches that chemisorb onto the iron surface in specific orientations, enabling the alkyl chains to form an inert cushion at the steel/steel interface. Lubrication occurs thanks to this chemical inert buffer region, which effectively separates the metal surfaces realizing a beneficial friction and wear reducing tribofilm, with a clear dependence on the chain length. These findings by a combined experimental-computational approach provide valuable insights for the development of sustainable lubricants, advancing the field of green tribology.

1. Introduction

The current trend toward fossil fuel conservation and environmental protection is driving tribologists to explore alternatives to traditional fuel-based lubricants. Polyalkylene glycol (PAG) is considered as a promising candidate for engine oil formulations, offering superior friction-reducing and load-bearing capabilities compared to conventional mineral-based and synthetic oils [1,2]. Additionally, PAG aqueous solutions can form hydrated films on ceramics, helping the achievement of superlubricity (coefficient of friction, CoF <0.01) in both the mixed lubrication ($\lambda = 2.4$) and elastohydrodynamic lubrication regimes [3].

However, when PAG is directly used to lubricate steel surfaces, additives such as MoS_2 and WS_2 quantum dots are required to achieve an ultralow CoF $\leq$0.1 [4]. These additives promote the formation of a protective tribofilm on steel, avoiding direct metal-to-metal contact. Nanosized MoS_2 deposited on graphene is an efficient additive for PAG, creating low-friction layers on steel surfaces [5]. Apart from Mo-based additives, hydroquinone bis (diphenyl phosphate) has also proven to be an excellent anti-wear agent for PAG, enabling the formation of a polyether-containing tribofilm [6].

* Corresponding author.
** Corresponding author.
E-mail addresses: clelia.righi@unibo.it (M. Clelia Righi), maria-isabel.de-barros@ec-lyon.fr (M.-I. De Barros Bouchet).

https://doi.org/10.1016/j.mtnano.2025.100629
Received 29 January 2025; Received in revised form 7 April 2025; Accepted 23 April 2025
Available online 24 April 2025

To broaden the choice of additives for PAG, we have extensively investigated the tribological performance of gallate molecules through both experimental studies and molecular dynamics simulations using machine learning interaction potentials (MLIP) with Density Functional Theory (DFT) accuracy. Gallates are attractive due to their abundance, renewability, eco-friendliness and antioxidant properties. For instance, gallic acid is a natural component found in sumac, tea and oak. Known for its oxygen scavenging ability, gallic acid is used in the medical treatment of cancer [7] and cardiovascular and inflammatory diseases [8]. Additionally, gallic acid and gallates family are also applied in cosmetic [9] and food industries [10] as antioxidant agents. In lubricant applications, gallate molecules such as propyl gallate [11] have been used as antioxidant agents in vegetable oils to increase their stability. For example, propyl gallate in B30 (a blend of 30 % biodiesel in diesel) results in the formation of an ester-based tribo-film reducing both friction and wear [12]. Gallates like 2-octyldodecyl gallate can also modify TiO_2 nanoparticles, improving dispersion stability and lowering friction [13]. Furthermore, by replacing the hydrogen atoms of gallic acid with alkyl chains, these gallate derivatives can be used directly as lubricants. Among them, substituting hydrogen atoms of phenolic hydroxyl groups with propyl chain and the hydrogen atom of the carboxylic group with dodecyl chain is the most efficient way to obtain low friction [14].

The role of the alkyl chains and the underlying friction reduction key mechanisms are unraveled exploring how gallate molecules interact with iron surfaces by means of DFT calculations and MLIP molecular dynamics simulations. First, the formation of a stable self-assembled monolayer (SAM) is revealed, triggered by molecules chemisorbed following the tribochemically activated dissociation of terminal OHs which promotes the creation of strong Fe-O-C bridges between the surface and the aromatic ring of the molecules which, as a results, adsorb in the upright orientation. The SAM is further stabilized by hydrogen bonding and vdW attraction between adjacent molecules. Second, following the dynamics, even in harsh tribological conditions, shows that these SAMs can withstand local loads of several GPa, with the alkyl chains forming a cushion, inert, region that keeps apart the most reactive parts of the molecules and the surfaces. This way, sliding is dominated by vdW interactions between the alkyl chains, thus substantially reducing friction and wear at the iron-iron interface. In agreement with experimental findings, the greatest reduction in friction is obtained for gallate molecules with longer alkyl chains.

This research pushes forward the application of gallate molecules in tribology, revealing their potential as efficient friction modifier and wear inhibitor in PAG-based aqueous solution. Reciprocating tests were conducted to evaluate the effect of gallate chain length on tribological behavior, being the solubility of the molecule successfully maintained within the adopted liquid solution The two most outstanding gallates, octyl gallate and lauryl gallate, were subsequently selected for MTM tests to evaluate their performance across a wide speeds range. X-ray Auger electron spectroscopy (XAES) and atomic force microscopy (AFM) analyses unveiled the underlying lubrication mechanisms. This study not only expands the selection of additive for PAG-based solutions but also addresses their limitations by utilizing robust gallate molecules that form stable layers on steel surface.

2. Experimental & computational sections

2.1. Materials & liquid preparations

For the tests conducted using the reciprocating tribometer, steel balls and discs were purchased from PCS instruments (London, UK) with surface roughness values of 19.7 and 4.4 nm, respectively. The steel balls have a diameter of 12.7 mm. As for steel specimens used in the mini-traction machine (MTM), they were also bought from PCS instruments. However, the balls in this setup have of 19.5 mm, with surface roughness values of 8.2 nm for the balls and 3.1 nm for the discs. All the information about the samples is summarized in Table 1.

The liquid base lubricant, named “331” in the following, is prepared by mixing three components: PAG (Breox 75w 55000), diethylene glycol and distilled water in a 3:3:1 ratio. Breox 75w 55000 was purchased from BASF (Ludwigshafen am Rhein, Germany) and diethylene glycol (purity ≥99 %) was sourced from Sigma-Aldrich (St. Louis, USA). Before use, the mixture was magnetically stirred for 10 min to ensure homogeneity. As a non-flammable and biodegradable hydraulic fluid, “331” is currently used in industries such as mining, agriculture, tunneling and hydraulic pumps.

Additives such as gallic acid (GA), propyl gallate (PG), butyl gallate (BG), octyl gallate (OG) and lauryl gallate (LG) were purchased from Sigma-Aldrich, each with a purity ≥99 %. Due to the poor solubility of gallates in “331”, we used TEA (triethanolamine) as a solubilizer in this study. TEA was provided by TotalEnergies (Courbevoie, France). The molecular structures of all compounds are shown in Fig. 1.

To dissolve the additives, 0.5 wt% TEA was added to “331”, and the mixture was magnetically stirred for 10 min. The viscosity of “331” + 0.5 wt% TEA at 25 °C was measured at 261 mPa s. Subsequently, 1 wt% of each gallate additive was added into the mixture. The solution was then heated to 60 °C and magnetically stirred for an additional 15 min. Before use, the final solution was cooled to ambient temperature. All prepared solutions were optically transparent, with corresponding photos shown in Fig. 1c. The base solution of “331” + 0.5 wt% TEA, as well as the solutions containing OG and LG, remained colorless. In contrast, the addition of GA and PG turned the solutions light yellow, while the introduction of BG resulted in a light pink color.

2.2. Tribological experiments

A first set of tribotests was conducted using a reciprocating tribometer in a ball-on-disk configuration [15]. A normal force of 10 N was applied to the disk, resulting in a maximum Hertzian pressure of 860 MPa and a contact diameter of 148 μm, as calculated based on [16]. The sliding speed on the ball side was controlled by a mechanical arm following a sine function, with a maximum speed of 3 mm/s at the midpoint of the track. All tests were performed three times at 25 °C under boundary lubrication regime.

The second set of tests was performed using a Mini-Traction Machine (MTM, PCS instruments, London, UK) allowing to test lubricant tribological performance over a wide range of speeds. The test protocol was divided into five steps. All steps were conducted at a temperature of 25 °C, with a normal force of 35 N and a slide-to-roll ratio of 100 %. Two timed steps were performed at speeds of 250 mm/s and 10 mm/s, each for 20 min (Fig. 2). Before and after a timed step, a Stribeck curve was systematically obtained, covering speeds from 5 mm/s to 2500 mm/s.

Table 1
Characteristics of body and counter-body materials.

	Supplier	Diameter (mm)	Elastic modulus (GPa)	Poisson ratio	Surface roughness (nm)	Hardness (GPa)
Steel ball	PCS instruments	12.7	210	0.3	19.7	8.3
Steel disk	PCS instruments	–	210	0.3	4.4	8.3
Steel ball (MTM)	PCS instruments	19.5	210	0.3	8.2	8.3
Steel disk (MTM)	PCS instruments	–	210	0.3	3.1	8.3

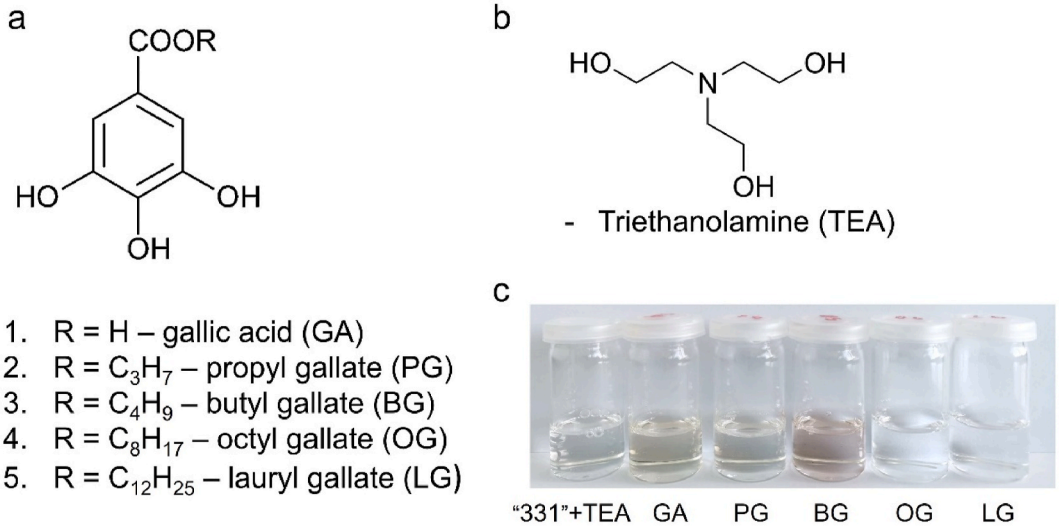

Fig. 1. Molecular structures of **(a)** GA, PG, BG, OG, LG and **(b)** TEA. **(c)** Photos of the prepared solution after cooling to ambient temperature.

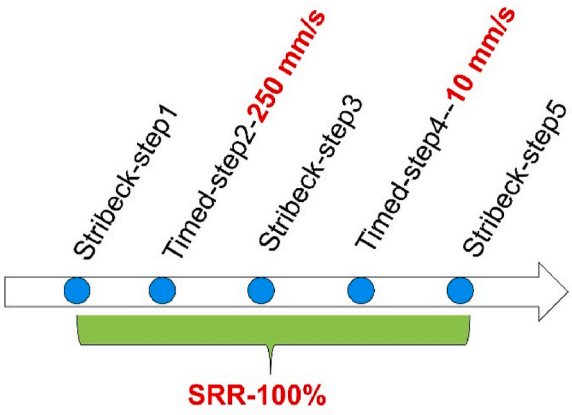

Fig. 2. Test protocol of MTM with five steps.

2.3. Surface analysis

After rinsing the worn steel surfaces with ethanol, wear scars were imaged by digital microscopy (VHX-6000, Keyence, Osaka, Japan). Topographic information such as wear depth, wear volume and surface roughness (Sa), were quantified using an interferometer (ContourGT-X, Bruker, Billerica, USA). Surface roughness (Sa) information was obtained from an area of 126 × 95 mm^2. The wear curvature radius was also acquired with the interferometer.

The top-surface chemistry was investigated using X-ray photoelectron spectroscopy (XPS) and X-ray-induced Auger electron spectroscopy (XAES). Both analytical techniques were powered by a ULVAC-PHI Versa Probe II spectrometer equipped with an Al Kα source (1486.6 eV). Photoelectron and Auger electron signals were collected from a 50 × 50 μm^2 area at a take-off angle of 45° and a pass energy of 23.5 eV. The XPS and XAES spectra were treated using Multipack software.

Deeper information was recorded using Raman spectroscopy (Invia™ confocal Raman spectroscopy, Renishaw, Gloucestershire, UK). A 633 nm laser was employed, and the laser power was maintained below 10 mW to avoid surface modification.

High-resolution topography information was further investigated using atomic force microscopy (AFM). AFM analysis was carried out on a Park NX 10 (Park Systems, Suwon, South Korea) with RESP tips (contact tips with k = 0.9 N/m) purchased from Bruker (Massachusetts, USA). The height profile and lateral force were recorded in contact mode, while the adhesion force was recorded in pin-point mode. The AFM tip remained in contact with the steel samples during the mode shifting, ensuring that the height profile, lateral force, and adhesion force were recorded in the same area within a water environment to minimize the impact of capillary forces on adhesion. Friction force was obtained from the lateral force signal by taking half the difference between the forward and backward scan signals. Although lateral force calibration was not performed, all experiments were conducted using the same tip and optical adjustments, allowing direct comparison of the obtained values.

2.4. Ab initio calculations and molecular dynamics simulations with machine learning interaction potentials

Steel based surfaces present several types of oxide with the degree of iron oxidation decreasing while nearing the metal substrate. In tribological conditions however, part of the superficial oxides will be removed and molecules easily come in direct contact even with the pure iron surface, which is much more reactive and can significantly favor molecule chemisorption [17] with respect to iron hydroxides/oxides. Thus, it can be expected that the most beneficial effect of the additives would be in alleviating direct Fe-Fe contacts and the computational work here has been focused on the simulation of an iron substrate in the presence of the gallate molecules to investigate the specific role of the alkyl chain length. A*b initio* calculations were performed for systems with four different gallate molecules (PG, BG, OG, and LG) adsorbed on Fe (110), used as representative of the native steel surface, within a 3 × 2 supercell (14.20 × 12.05 Å) with a thickness of 4 atomic layers, using spin–polarized density functional theory (DFT) implemented in VASP package version 6.3.2 [18] using the projector–augmented wave (PAW) method with the Perdew–Burke–Ernzerhof (PBE) functional [19] and the DFT–D2 method of Grimme [20,21] to account for the van der Waals (vdW) dispersion interactions. The detailed setup for the DFT calculations can be found in Ref. [22].

A Deep Neural Network (DNN) machine learning interaction potential (MLIP) was trained using the DeepMD–kit package with the DeepPot– SE (Deep Potential–Smooth Edition) model [23]. To effectively improve the DNN potential, additional data frames were generated through an active learning approach [24,25] employing DFT based static and *ab initio* molecular dynamics (AIMD) calculations. Details about the AIMD simulations, the training process, and the active learning approach to generate more data for the MLIP training are presented elsewhere [22,25]. Molecular dynamics simulations with the DNN potential were performed with Lammps [26] with a time step of 0.1

fs in the NVT ensemble at 300 K using separate Nosé-Hoover thermostats for each of the iron slabs. Tribological conditions were simulated imposing a fixed relative velocity of $v = 50$ m/s along the x direction between the uppermost and the bottom-most layer of iron atoms at different applied loads ranging from 0.5 GPa to 2.5 GPa (see Fig. 3). Averages were performed over atomic configurations collected at every 10 fs along the simulated trajectories.

3. Results

3.1. Gallates performance in reciprocating sliding test configuration

In tests performed with the reciprocating tribometer, the formulation of base oil "331" added with 0.5 wt% TEA exhibited a gradual increase in the friction coefficient from 0.15 to 0.22 over time. Such a high friction coefficient at low sliding speeds is not practical for applications. Introducing GA, PG and BG into "331" + TEA reduces the CoF during the running-in period; however, it eventually approaches the base oil value and remains above 0.12. In contrast, the addition of OG and LG significantly reduces the steady CoF to a value ≤ 0.06. Notably, this ultralow friction state is achieved early in the test during the running-in period. When comparing OG and LG, LG demonstrates greater efficiency in friction reduction than OG stabilizing CoF at approximately 0.04, while the steady CoF of OG is around 0.06.

On the other hand, friction induces topography changes on steel surfaces. After lubrication with "331" + TEA, the steel ball is fully covered with grey Fe_3O_4 species, as indicated by the characteristic Raman peak of Fe_3O_4 detected at 670 cm^{-1} [27] (Fig. 5g). The wear scar diameter on the steel ball is 212 μm (Fig. 5a) corresponding to a wear volume is −2678 μm^3 (Fig. 4b), indicating that the Fe_3O_4 species exceeds the material loss due to shear. On the contrary, the disk side experiences significant wear, with a wear volume of 45898 μm^3. The addition of GA, PG, and BG alters the topography of steel surfaces (Fig. 5b–d) and forms Fe_3O_4 species (Fig. 5g) in the wear track. However, these three additives do not reduce the total wear volume of the balls and disks. Especially, in the case of GA, the wear diameter on the steel ball is enlarged to 346 μm (Fig. 5b), with a corresponding wear volume of 132180 μm^3 (Fig. 4b). In addition to Fe_3O_4, the D and G peaks of amorphous carbon are detected at 1323 cm^{-1} and 1571 cm^{-1} [28]. An additional peak is recorded at 1470 cm^{-1}, which is also present in hydroquinone [29].

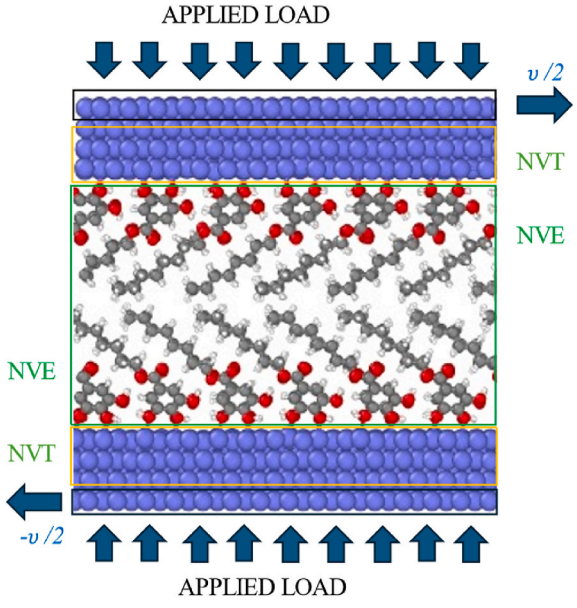

Fig. 3. Model with two opposing gallate monolayers confined between two Fe (110) substrates for MLIP molecular dynamics simulations in tribological conditions.

Following the CoF reduction with the addition of OG or LG, the total wear volume decreases significantly with these two additives (Fig. 4b). In the case of OG lubrication, the steel ball is found to have a wear diameter of 184 μm (Fig. 5e) and a material loss of 8873 μm^3, while no measurable wear is observed on the disk side. For the LG case, the wear diameter on the steel ball is 149 μm (Fig. 5f), with no measurable wear detected on either side. It is noteworthy that the Hertzian diameter is 148 μm in this context. Upon closer examination of optical images, light yellow species are found (not shown here) inside the wear track for both cases, which correlates well with the formation of Fe_3O_4 and Fe_2O_3 peaks detected by Raman at 217, 286, 402, and 1321 cm^{-1} (Fig. 5g) [30].

XPS analysis revealed the chemical distribution of the steel top surface. The as-received steel surface contained only carbon, oxygen and iron, as expected. However, after the friction tests, nitrogen was found on all steel surfaces (Table 2), indicating that TEA contributes to changes in surface chemistry, as it is the only nitrogen source present. Comparing the cases with gallate molecules GA to OG, the nitrogen content decreases as the carbon amount in the alkyl chains increases. The nitrogen content of the LG lubrication case is similar to that of OG, suggesting that both OG and LG may inhibit the adherence of TEA to the steel surfaces. Concerning iron content, the use of GA significantly reduces iron content from 9.9 % to 1.8 % compared to the base liquid lubrication case. Correspondingly, the GA case exhibits the highest carbon content among all analyses, which can be attributed to carbon species either being attached to or formed on the steel surface (Fig. 5g). Another noteworthy element is the relative decrease in the intensity of the C-O(H) contribution in the wear tracks lubricated by gallate compounds compared to the gallate powders. This could be due to the thermally activated breaking of the OH bonds, in particular during friction (Fig. S1).

The most significant difference between the gallate molecules is the alkyl chain length as shown by the XPS C1s core levels recorded on the powders through the relative intensities of the different contributions from C-C/C=C, C-O(H), O=C-O and pi/pi* (Fig. S1). XAES was also performed to quantify the length using the characteristic peak at approximately 261 eV, which represents the -$(CH_2$-$CH_2)_n$-structure [31]. Regarding XAES analysis of gallate powders, a remarkable peak is found at 261.2 eV for LG and 261.6 eV for OG (Fig. 6a). The peak location shifts to higher kinetic energy with a decrease in the alkyl chain length (Fig. 6d). This trend is also evident in the transition from LG to PG. For GA and PG, both exhibit peaks located at 263.1 eV. Conversely, OG and LG show the most prominent peak areas, represented as the area between the dashed line and the XAES spectrum from 259.6 to 265.6 eV (Fig. 6a). A declining trend in peak area is observed with a decrease in the number of carbons in the alkyl chain (Fig. 6c). For the GA case, the peak area is negligible, which aligns with the fact that GA does not possess a -$(CH_2$-$CH_2)_n$-linear chain.

Concerning the correlation between peak location/area and alkyl chain length, steel surfaces lubricated with different solutions exhibit a relationship similar to that of gallate powders (Fig. 6c and d). However, the peak locations after friction are generally about 0. 3 eV lower than those of the gallate powders. As for the peak areas after friction, they are almost identical to the values observed for the gallate powders. These similarities strongly suggest that gallate molecules are firmly attached to the steel surfaces. Consequently, the alkyl chain features, such as the peak position and area of the -$(CH_2$-$CH_2)_n$-group, are preserved when analyzing the rubbed steel surfaces. It is important to note that these alkyl chain features cannot originate from "331" or TEA, as the XAES spectrum of steel lubricated with this solution does not exhibit a remarkable -$(CH_2$-$CH_2)_n$-signal near 261 eV, and their peak shape resembles that of GA case, which lacks alkyl chains.

XAES results confirm that gallate molecules are attached to steel surfaces. To further investigate the distribution of these molecules, AFM was employed. For the steel surface lubricated with "331" + TEA,

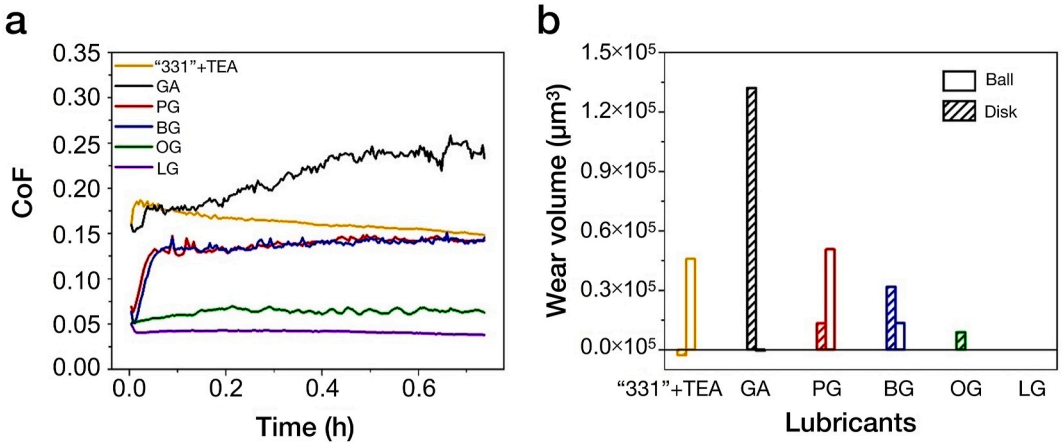

Fig. 4. Tribological tests conducted using the reciprocating tribometer: (**a**) Friction curve as a function of time. (**b**) Wear volumes of the balls and corresponding to each lubricant type.

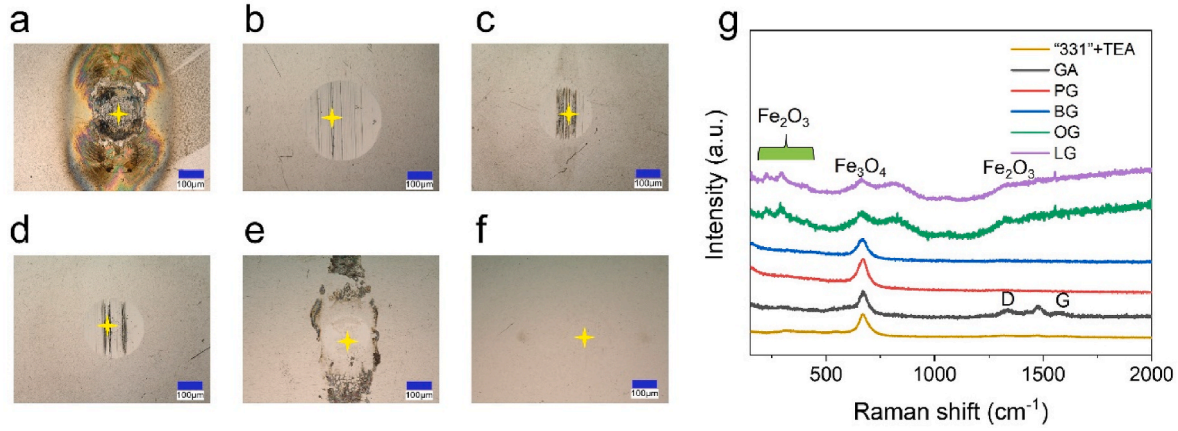

Fig. 5. Optical images of steel balls lubricated with "331" + TEA: (**a**) without additive; (**b**) with GA; (**c**) with PG; (**d**) with BG; (**e**) with OG; (**f**) with LG. The blue scale bar represents 100 μm. (**g**) Raman spectra of steel wear after lubrication with different solutions, with analysis locations marked by yellow stars (**a-f**).

Table 2
Elemental composition of the steel surface after friction test, as determined from XPS survey spectra.

	C1s	O1s	Fe2p3/2	N1s
(331+TEA)	50.2	37.7	9.9	2.2
+GA	63.5	32.1	1.8	2.6
+PG	43.3	42.0	13.5	1.2
+BG	42.2	41.3	15.5	1.0
+OG	39.8	46.8	12.8	0.6
+LG	46.4	41.8	11.1	0.7

scratches of approximately 30 μm were observed (Fig. 7a). Despite this significant difference in topography, no corresponding variation in friction and adhesion force distribution was detected within the scratches; the friction and adhesion forces were similar to those in areas outside the scratches. This lack of correlation between surface height and force was also observed in the cases of GA, PG, and BG (not shown here).

Steel surfaces lubricated with OG and LG are covered by patches with an average height of approximately 10 nm (Fig. 7b and c), which are easily distinguishable from other areas due to their lower friction and adhesion forces. The OG-lubricated surface shows significantly higher patch coverage compared to the LG-lubricated surface. However, within these patches, the average friction is 0.054 V for the LG case and 0.065 V for the OG case. Additionally, the average adhesion force is 37 nN for LG and 42 nN for OG. These findings are consistent with performances obtained with the reciprocating tests, where LG lubrication demonstrates a lower CoF compared to OG.

In conclusion, XPS/XAES analyses demonstrate that gallate molecules have chemically bounded to steel surfaces and conserved their original alkyl chains during the reciprocating tests conducted at a reduced sliding speed range (maximum 3 mm/s). AFM further unveils that only OG and LG lubricant additives provide ultralow friction, low adhesion patches on steel surfaces, which are non-homogeneously distributed. Meanwhile, the patches created by LG exhibit lower friction compared to those formed by OG.

3.2. *Gallate performance in MTM test configuration*

MTM further investigates the lubricity of the base liquid and additives to extend their performance across a wide speed range. When the liquid base "331" + TEA lubricates a steel pair without undergoing a timed step, superlubricity is achieved (CoF $\leq$0.01) at rolling speeds above 150 mm/s (Fig. 8a). Even at rolling speeds below 20 mm/s, it can maintain a CoF around 0.08. However, its lubricity deteriorates at rolling speed $\leq$20 mm/s if the steel pair is subjected to a timed speed of 250 mm/s or 10 mm/s. The short-term rolling at a fixed speed results in a sudden increase of CoF when the rolling speed is $\leq$ 20 mm/s. For instance, after sliding at 10 mm/s, the CoF can reach 0.18 within the tested speed range.

The limitation of the practical application of "331" + TEA lies in its

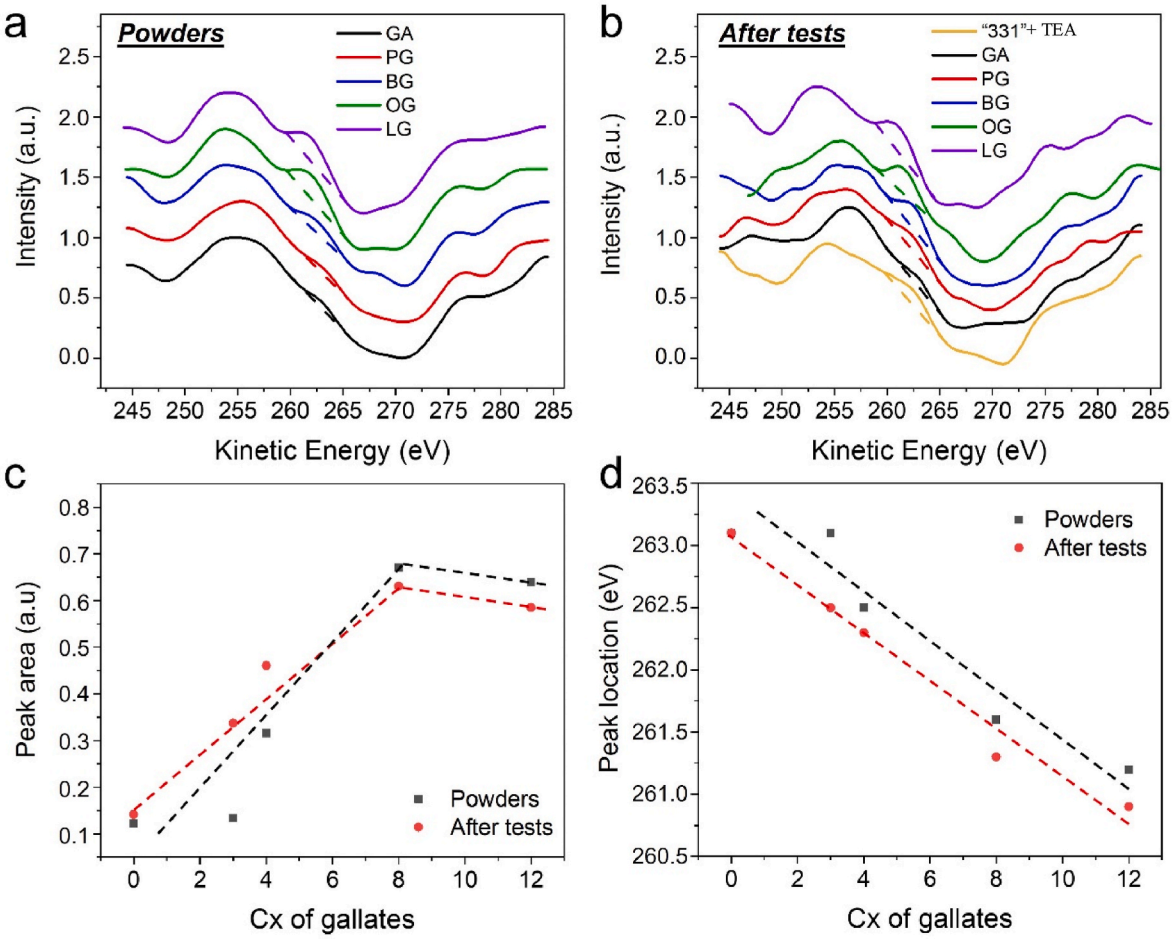

Fig. 6. The normalized CKLL first derivative: (**a**) for gallate molecule powders and (**b**) for steel wear tracks lubricated by different solutions. The dashed lines connect data points at 259.6 eV and 265.6 eV in KE. The area between the dashed line and the XAES spectrum between 259.6 eV and 265.6 in KE eV is referred to as the peak area. **c-d** correlation between (**c**) peak area and (**d**) peak location, and the carbon content in the alkyl chains of gallate molecules.

poor lubricity at low rolling speeds. Therefore, additives are expected to preserve the low friction of the water-based liquid at rolling speeds ≥150 mm/s while addressing the high friction issue at lower rolling speeds. The addition of OG and LG at 0.1 wt% (noting that higher amounts of gallates, such as 1 wt%, can slightly increase CoF at rolling speeds ≥1500 mm/s) fulfills these requirements. They maintain a CoF below 0.003 at rolling speeds above 250 mm/s and ensure CoF ≤0.07 at rolling speeds below 250 mm/s (Fig. 8b and c). Their addition significantly changes the Stribeck curve, producing a plateau-like curve for rolling speeds below 30 mm/s. Additionally, timed steps at 250 mm/s and 10 mm/s have no impact on the final shape of the Stribeck curve. Therefore, the lubricity of "331" + TEA is enhanced by the OG/LG addition, resulting in a formulated lubricant remains exceptionally stable, even under severe conditions (low rolling speeds).

3.3. Ab initio (DFT) calculation of the adsorption of gallate molecules on iron surface

The minimum energy configurations of (PG, BG, OG and LG) gallates molecules adsorbed on the Fe (110) surface were investigated *ab initio* to draw initial ideas about the strength and configurations of the Fe-gallate interactions. A single molecule was initially geometrically optimized at several adsorption sites with either a perpendicular or a parallel orientation of the aromatic ring on the iron (110) surface (Fig. 9a and b). For intact molecules DFT adsorption energies are lower with the aromatic ring parallel to the surface, thanks to the formation of multiple chemical bonds between surface iron atoms and the carbon atoms of the ring (Fig. 9a). However, it is known that surfactant molecules can, even spontaneously, deprotonate when adsorbed on iron/iron oxides surfaces [32]. It is well-known that the iron surface is highly catalytic [33] and facilitates the spontaneous dissociation of the OH [34]. Deprotonation is thermally activated already at 300 K, as observed for the BG molecule [22]. Indeed much more favorable adsorption energies are found for all four molecules (Fig. 9g insert), when the perpendicular oriented adsorption is considered, allowing for the removal of two hydrogen atoms from the OH groups at the base of the molecule. In particular, the dissociative adsorption promotes the formation at the interface of multiple, direct, Fe-O-C chemical bridges that stabilize the aromatic ring perpendicularly to the surface (Fig. 9c), a finding which is also in a good agreement with the XPS spectra measured experimentally (Fig. S1). On the contrary, the occurrence of deprotonation of the OH groups cannot be observed with reference ReaxFF models [35] even under high loads and sliding in harsh tribological conditions [22], underlying the importance of quantum accurate description of the molecule-surface interaction which is achieved by DFT and inherited by the deep neural network potential.

Moreover, thanks to this molecular orientation, there is a sizable energy gain when more molecules are added (Fig. 9d, e, f) with the formation of an ordered monolayer structure [36,37], which is further stabilized both by the establishment of hydrogen bonding between molecules and by the attractive vdW interactions between the alkyl chains. The monotonic decrease of adsorption energies per molecule is shown in Fig. 9g for the undissociated case. The energy gain is higher the longer is the length of the alkyl chain of the molecule and, for OG and

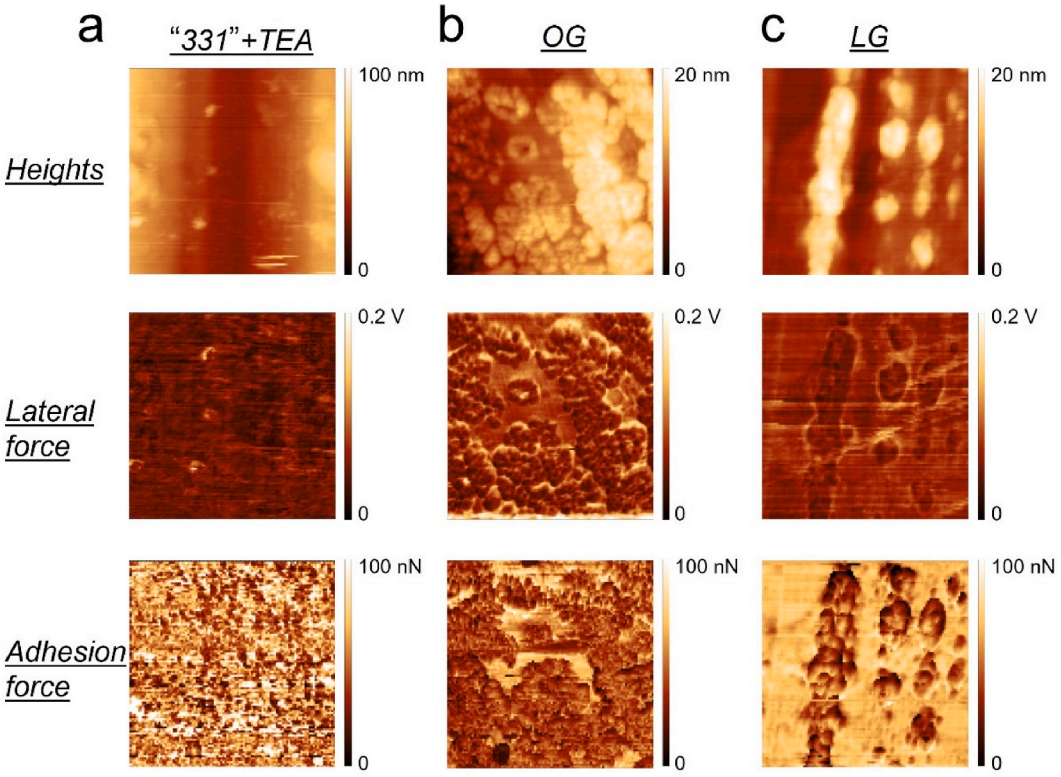

Fig. 7. AFM analysis on steel surface lubricated by (**a**) "331" + TEA, (**b**) "331" + TEA + OG and (**c**) "331" + TEA + LG. Their heights (top), lateral force (middle), and adhesion force (bottom) distribution in an area of 2.5 × 2.5 μm^2 are listed.

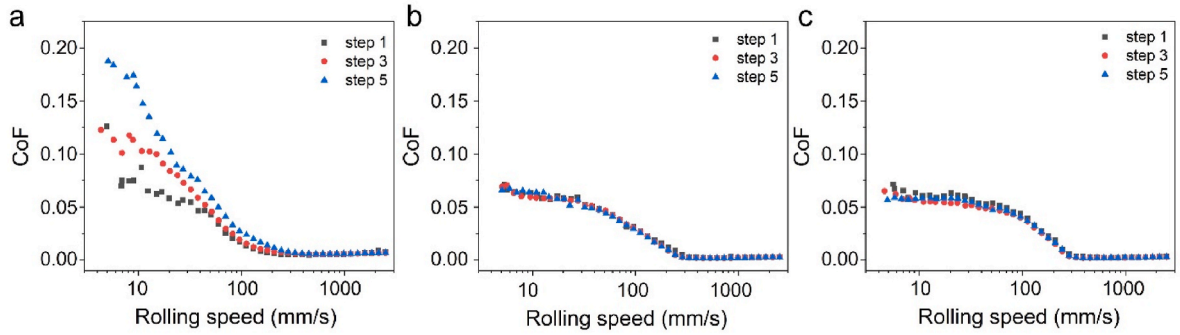

Fig. 8. Tribological tests performed on MTM: (**a**) "331" + TEA, (**b**) "331" + TEA + 0.1 wt% OG and (**c**) "331" + TEA + 0.1 wt% LG. Steps 1 and 3 are the Stribeck curves before and after a timed step at 250 mm/s respectively. Step 5 is the Stribeck curve after a timed step at 10 mm/s.

LG, it can compensate and even surpass the energy advantage of the single molecule parallel adsorption (Fig. 9g insert). These results testify the presence of a competition between these two preferred adsorption geometries, with the case of the molecule aromatic ring parallel to the iron surface favored at low coverages in the absence of dissociations while, with increasing molecular concentration, the perpendicular one becomes more and more favorable the longer is the alkyl chain leading, after deprotonation, to the formation of stable ordered SAMs.

The coverage of the Fe (110) surface does not depends from the alkyl chain length and a full coverage is achieved at a density of 0.035 molecules per Å^2 (for the considered systems corresponding to six molecules in the 3 × 2 supercell [22]), where one observes the formation of an ordered self-assembled monolayer (SAM), well matched with the periodicity of the Fe (110) surface (Fig. 9f).

3.4. (MLIP) molecular dynamics simulation in tribological conditions

To identify the nature of the underlying mechanisms responsible for the tribological performances of gallate compounds, and particularly the effect of the alkyl chain length, numerical simulations were performed with an ad-hoc trained DNN potential (details of the training are given in the SI; see Fig. S2 and Fig. S3). The initial conditions of the atomic configurations for the MLIP-MD simulations were built starting with the full coverage SAM adsorbed on the Fe (110) surface, obtained by replicating the optimized DFT supercell with 6 adsorbed molecules in order to obtain a larger MD supercell with a surface area of 42.6 × 36.15 Å^2 and each of the two opposing SAMs containing 54 molecules (Fig. 3). The models with 66 % coverage (36 molecules per SAM) were then obtained by removing 1/3 of molecules. The total number of iron atoms staying fixed to 2160 in both systems.

Frictional properties of the Fe-gallate systems with different chain lengths are presented in Fig. 10 as a function of the applied load for two

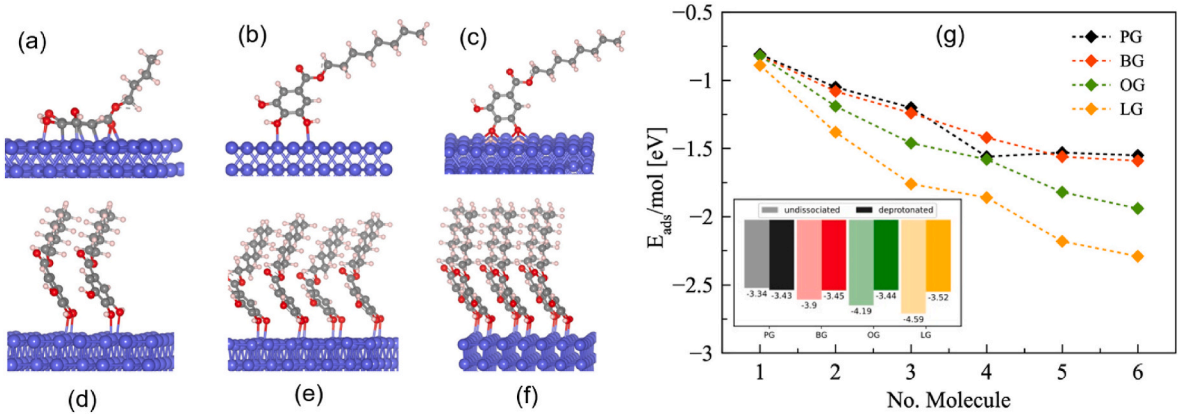

Fig. 9. Stable structures of gallate adsorption on Fe(110) surface: (a) BG parallel adsorption, (b) OG intact molecule perpendicular adsorption, (c) dissociative adsorption for the OG molecule, (d, e, f) perpendicular adsorption of 2-4-6 gallate molecules. (g) Adsorption energies per molecule as a function of the number of molecules in the 3x2 supercell with, in the insert, the comparison between the single molecule adsorption energies of the undissociated in the parallel configuration and of the twice deprotonated in the perpendicular configuration.

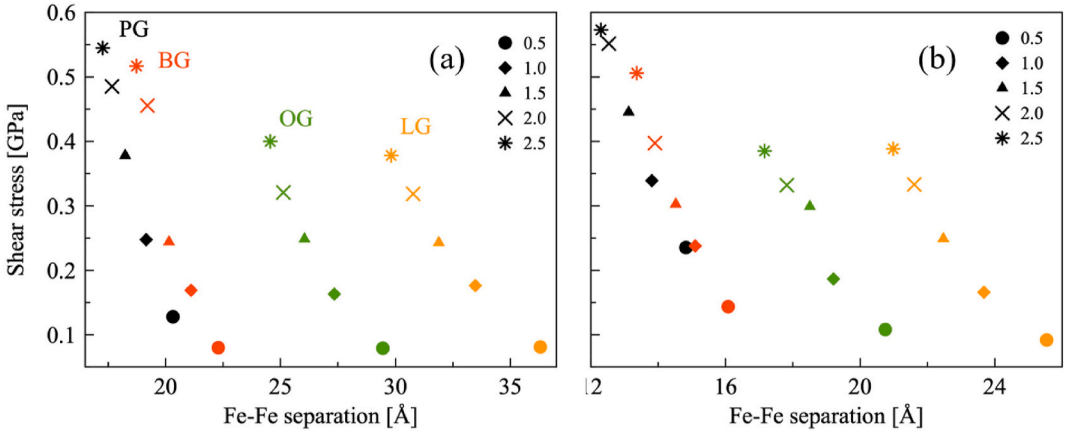

Fig. 10. Frictional properties of Fe-gallate systems with different chain lengths: resistive force per unit area as a function of the Fe-Fe separation distances at full (a) and 66 % (b) coverage. The applied pressure in GPa is specified in the symbol legends.

different coverages. The Fe-Fe separation distances between the two iron substrates are relatively large for all gallate molecules. The Fe-Fe gaps range from 16 Å to 36 Å for 100 % coverage and from 12 Å to 26 Å for 66 % coverage with a quasi-linear inverse dependence on the applied load, and a monotonic increase with the chain length. The most significant reduction is found with the longer OG and LG chains as the applied load increases (Table S1). It is worth mentioning that the roughly estimated lengths of the molecules (as depicted in Fig. S4**)** are ~10.04, 10.97, 15.80 and 20.75 Å for PG, BG, OG, and LG, respectively. At 100 % coverage the relative ratios of these lengths are well reflected in the behavior of the separation distances for the different molecules, a clear sign of the stability of the ordered SAM layers under tribological conditions.

Resistive forces per unit area present not only the expected monotonic increase, roughly proportional to the applied load, but also a clear dependence on the alkyl chain length of the molecules (Fig. 10). At full coverage with the lowest applied pressures (0.5 GPa) a remarkably low friction was obtained for all gallate molecules, with a slightly higher value only for the PG system. Indeed, these roughly similar, low, values for the frictional forces at the lowest load can be explained by a friction mechanism dominated by the Pauli repulsion and the weak vdW interaction between the well-ordered alkyl chains in the SAMs. As the applied load increases, the friction increases in a more pronounced way for PG and BG molecules, but only in a significantly slower way for the OG and LG molecules. For the latter there appear to be only minor differences between the frictional forces for the full and the 66 % coverages, with a much more pronounced increase in friction values observed for the shorter chain molecules, PG and BG, especially at lower loads.

Overall, the MLIP-MD results show that for the longer chains (OG and LG) friction remains relatively low in a remarkably consistent way for all the loads in the studied range and independently of the SAM coverage. The shorter chains (BG and PG), on the contrary, can only provide some degree of friction reduction with ordered SAMs at full coverage and for the mildest applied pressures, but they fail doing so at high applied loads, indeed at all loads in the 66 % coverage case. The MLIP molecular dynamics results confirm, well in line with experimental findings, the occurrence of a beneficial chain length effect on friction. This effect becomes more pronounced when the molecules are loosely packed, i.e. when it is no longer possible to observe a stable, ordered SAM.

To understand more in depth the underlying mechanisms leading to higher friction reductions for the long chains and the different behavior at lower coverage densities, it is important to analyze in detail the structures of the Fe-gallate systems under sliding conditions. The system snapshots in the upper panels of Fig. 11a–d are taken at the sliding time of 500 ps, for the PG and LG respectively at full and 66 % coverage, with 1 GPa applied pressure. For all systems, molecular adhesion is well conserved during the sliding, stabilized by the Fe-O-C bridges resulting from the deprotonation of two initial Fe-OH bonds. At full coverage, apart rare exceptions, for the vast majority of the molecules the aromatic

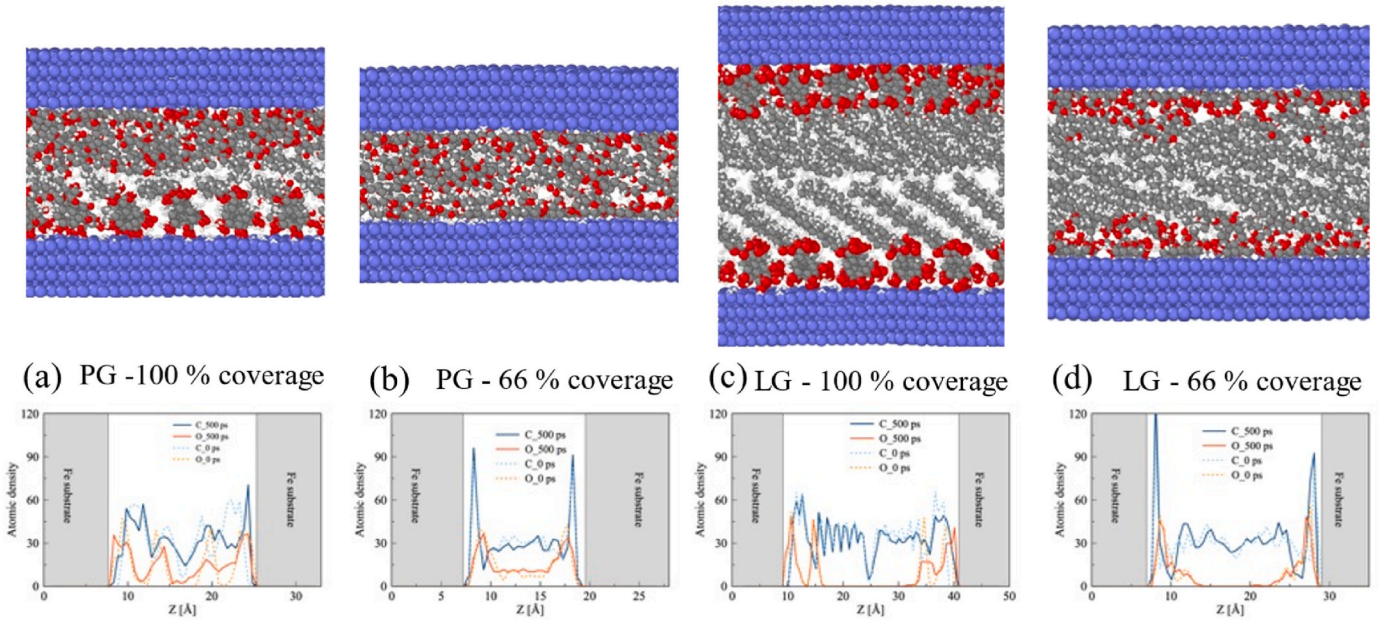

Fig. 11. Snapshots of Fe-gallate sliding systems at 1 GPa and 500 ps (**a-d**) and the corresponding atomic density profiles (**e-h**), obtained averaging over 10 ps after the first 500 ps of the sliding process.

rings stand perpendicularly while the last three/four -CH_x groups of the alkyl chains become flattened to better accommodate with compression and sliding. This behavior is featured by sharper peaks in the density profiles located near the iron substrates (Fig. 11a–d, lower panels). These flat layers remain ordered and evenly distributed, in both the short-chain (PG and BG) and, more pronounced, in the long-chain (OG and LG) systems, and they can be assumed to be responsible for load bearing and friction reduction.

The most significant structural difference between the short and the long chain systems can be found in the vertical distribution of the oxygen atoms. For LG (and OG) peaks in the density of the oxygen remain well separated by the, flattened, alkyl chains, while for PG (and BG) there is no gap. In particular, in the short-chain systems, much shorter distances are found between the highest C-O groups of the molecule in the opposing monolayers and even the distances of the oxygen atoms of one monolayer from the iron atoms of the opposed surface, a situation that becomes more pronounced as the load increases. As a result, stronger chemical reactive interactions become more frequent between the opposing layers, particularly in the case of PG. The greater increase of friction observed for the short-chain systems can be primarily associated with these stronger interactions across the interface, that cannot take place in the longer chain systems where the alkyl chains, either in an ordered or even somewhat disordered fashion, are able to sustain an effective separation at the interface with weaker vdW interactions dominating the friction behavior.

The reduction of the Fe-Fe interfacial distances at low coverage shown in Fig. 11 can be associated with the loss of the perpendicular orientation of part of the gallate molecules. Their aromatic rings adsorb onto the Fe surface filling space left by the removal of gallate molecules previously adjacent in the 100 %-coverage systems. There is additional disorder in the alkyl chain with a consequent loss of intermolecular hydrogen bonding.

4. Discussion

It is worth mentioning that without TEA, only 1 wt% GA, PG, and BG can be fully dissolved inside “331”. This is because increasing alkyl chain length results in a greater hydrophobicity of the molecules. Given that “331” is a polar liquid, it is reasonable that a longer alkyl chain length would negatively impact the solubility of gallate molecules in “331”. However, tribological tests (Fig. 4a) have demonstrated that adding GA, PG, and BG to “331” + TEA does not sufficiently reduce friction and wear. This indicates that the gallate core and gallate molecules with short alkyl chains ($C_x < C_8$) are not robust enough to bear the load and maintain separation between the two surfaces. In contrast, the addition of OG and LG significantly ameliorates the friction and wear performances of the water-based lubricant (Fig. 4a). This finding is consistent with other studies on the effect of fatty acid chain length on friction [38], which report a pronounced friction reduction when the alkyl chain length is above C_6.

XAES results show that alkyl chains remain present on steel surfaces after friction even under severe loading condition. The gallate molecules are expected to anchor onto the steel surfaces through chemisorption of the polar core and physisorption of the alkyl chain. Polar groups, such as hydroxyl (OH), have stronger affinity for steel surfaces compared to non-polar groups like CH_3 [39], and gallate polar core contains 3 OH-functions. Indeed, gallic acid is frequently used as a corrosion inhibitor for steel, as it chemically adsorbs onto steel surfaces and forms highly stable complexes with iron [40]. This process also produces hydroxyquinone due to the oxidation of gallic acid, which explains the Raman peak observed at 1470 cm^{-1}.

The lubrication regime calculation further supports the crucial role of gallate molecules in lubricating the contact. For instance, in tests performed with the reciprocating tribometer at 3 mm/s and 25 °C, Table 3 shows that, regardless of the addition of OG or LG, the final

Table 3
Relevant parameters for tests conducted with reciprocating tribometers at 3 mm/s and 25 °C. The Lambda (λ) value represents the ratio between composite surface roughness and the liquid film thickness, with the latter calculated using the Nijenbanning-Venner-Moes equations [41]. The pressure-viscosity coefficient of “331” + 0.5 wt% TEA is assumed to be 7 GPa^{-1} [42].

	OG		LG	
	Ball	Disk	Ball	Disk
Roughness **after tests** (nm)	53.9	8.6	11.0	4.5
Radius of wear curvature **after tests** (mm)	14.1	–	6.8	–
Liquid film thickness (nm)	10.0		6.8	
λ	0.18		0.57	

Lambda (λ) ratio, calculated at the end of the friction experiment, remains well below unity, indicating that friction arises from the contact between asperities. Therefore, the remarkable friction-reducing properties of OG and LG under severe sliding and rolling/sliding conditions can be attributed to their ability to remain firmly anchored to the contacting asperities while maintaining a dense, orderly chain structuration, effectively keeping the opposing surfaces separated.

The friction reduction observed in the MLIP molecular dynamics results in Fig. 10 highlights the importance of the alkyl chains with the longer chain OG and LG molecules outperforming the shorter PG and BG counterparts, in agreement with the experimental findings. The breaking of OH bonds to form direct Fe-O-C configurations, also observed in the XPS analysis, is fundamental to stabilize the upright orientation of the aromatic ring of the molecules in the SAM throughout the sliding process. As a result, friction reduction is commanded by the environment of the tightly packed alkyl chains [43], while the magnitudes of the resistive forces are relatively consistent among different chain lengths. Friction reduction is higher, with a lesser dependence on the chain length, when full coverage gallate SAMs are sandwiched between the two iron surfaces. This can be explained by the fact that the alkyl chains remain more tightly packed and present each other a more flattened surface. At lower coverages, the structure of the SAMs becomes somewhat disordered with part of the molecule adsorbed with the aromatic ring parallel to the surface. In these conditions, an effective friction reduction can only be attained with the longer chain molecules, OG and LG.

In summary, from the analyses of the molecular structures of the gallate systems under sliding conditions, we propose a mechanism of friction reduction which is based on the formation of a SAM in which the head group positions are stabilized by the formation of Fe-O-C chemical bonds that results from OH bond dissociation, with the alkyl chains playing the major role as friction supportive layer. The more ordered is the SAM the higher is the friction reduction. This property, in the cases studied here, is secured by the longer chains OG and LG molecules, which have been proven, in agreement with the experimental tribological tests, to provide better frictional performance, in all studied geometries, compared to the shorter chains BG and PG molecules.

5. Conclusions

This study presents an effective strategy to reduce friction and wear on steel substrates in PAG aqueous solutions (such as "331″) at low sliding speeds, achieved by the addition of organic gallate molecules. Significant reductions in both friction and wear are observed when the alkyl chain length of gallates is $\geq$ 8 carbon atoms, with C12 (lauryl gallate, LG) outperforming C8 (octyl gallate, OG) in lubricity. Specifically, the addition of OG to "331" + TEA results in a 73 % reduction in the coefficient of friction (CoF) and an 81 % reduction in wear, while LG eliminates measurable wear and achieves an 82 % reduction in CoF. Additionally, MTM testing demonstrates that the inclusion of either OG or LG in "331" + TEA preserves the low-friction characteristics of the water-based lubricant at high rolling speeds and makes friction nearly independent of rolling speed at values below 30 mm/s. The lubricity is stable and robust, as evidenced by the unchanged Stribeck curve even in the boundary lubrication regime.

As confirmed through XAES analysis, AFM imaging and DFT-accurate MLIP molecular dynamics simulations, the superior lubricity is attributed to the presence of long alkyl chains that form molecular layers strongly adsorbed onto the steel surface. These layers convert steel-to-steel contact into interactions between alkyl chains, where lubrication is facilitated by Pauli repulsion and weak van der Waals forces. Computational analysis further reveals that the deprotonation of the basal hydroxyl groups in gallate molecules is crucial for the strong adhesion of these molecular patches to the iron surfaces. These findings offer valuable insights for designing effective, eco-friendly water-based lubricants with enhanced tribological performance.

Declaration of competing interest

The authors declare that they have no known competing financial interests or personal relationships that could have appeared to influence the work reported in this paper.

Acknowledgments

M.C.R. and H.T.T. acknowledge the project “Advancing Solid Interface and Lubricants by First Principles Material Design (SLIDE)” that has received funding from the European Research Council (ERC) under the “European Union’s Horizon 2020 research and innovation program (Grant agreement No. 865633).” M.I.D.B.B. gratefully acknowledge the European Union and the Auvergne-Rhône-Alpes region for the funding of FEDER project, PLATEFORME TRIBLOGIE MOTEURS. MCR acknowledges support by ICSC–Centro Nazionale di Ricerca in High Performance Computing, Big Data and Quantum Computing, funded by European Union–Next Generation EU.

Appendix A. Supplementary data

Supplementary data to this article can be found online at https://doi.org/10.1016/j.mtnano.2025.100629.

Data availability

Data will be made available on request.

References

[1] A. Gangopadhyay, Z. Liu, S.J. Simko, S.L. Peczonczyk, J.B. Cuthbert, E.D. Hock, A. Erdemir, G. Ramirez, Friction and wear reduction mechanism of polyalkylene glycol-based engine oils, Tribol. Trans. 61 (4) (2018) 621–631, https://doi.org/10.1080/10402004.2017.1381286.

[2] D.E. Sander, C. Knauder, H. Allmaier, D.L. Baleur, P. Mallet, Friction reduction tested for a downsized diesel engine with low-viscosity lubricants including a novel polyalkylene glycol, Lubricants 5 (2) (2017) 9, https://doi.org/10.3390/lubricants5020009.

[3] H. Wang, Y. Liu, J. Li, J. Luo, Investigation of superlubricity achieved by polyalkylene glycol aqueous solutions, Adv. Mater. Interfac. 3 (19) (2016) 1600531.

[4] X. Wu, K. Gong, G. Zhao, W. Lou, X. Wang, W. Liu, MoS2/WS2 quantum dots as high-performance lubricant additive in polyalkylene glycol for steel/steel contact at elevated temperature, Adv. Mater. Interfac. 5 (1) (2018) 1700859, https://doi.org/10.1002/admi.201700859.

[5] K. Gong, X. Wu, G. Zhao, X. Wang, Nanosized MoS2 deposited on graphene as lubricant additive in polyalkylene glycol for steel/steel contact at elevated temperature, Tribol. Int. 110 (2017) 1–7, https://doi.org/10.1016/j.triboint.2017.01.024.

[6] G. Zhao, X. Wu, W. Li, X. Wang, Hydroquinone bis (diphenyl phosphate) as an antiwear/extreme pressure additive in polyalkylene glycol for steel/steel contacts at elevated temperature, Ind. Eng. Chem. Res. 52 (22) (2013) 7419–7424, https://doi.org/10.1021/ie4005578.

[7] Y. Jiang, J. Pei, Y. Zheng, Y.J. Miao, B.Z. Duan, L.F. Huang, Gallic acid: a potential anti-cancer agent, Chin. J. Integr. Med. (2021) 1–11, https://doi.org/10.1007/s11655-021-3345-2.

[8] J. Bai, Y. Zhang, C. Tang, Y. Hou, X. Ai, X. Chen, Y. Zhang, X. Wang, X. Meng, Gallic acid: pharmacological activities and molecular mechanisms involved in inflammation-related diseases, Biomed. Pharmacother. 133 (2021) 110985, https://doi.org/10.1016/j.biopha.2020.110985.

[9] A. Perez, D.A. Basketter, I.R. White, J. McFadden, Positive rates to propyl gallate on patch testing: a change in trend, Contact Derm 58 (1) (2008) 47–48, https://doi.org/10.1111/j.1600-0536.2007.01150.x.

[10] H. Hamishehkar, S. Khani, S. Kashanian, J. Ezzati Nazhad Dolatabadi, M. Eskandani, Geno-and cytotoxicity of propyl gallate food additive, Drug Chem. Toxicol. 37 (3) (2014) 241–246, https://doi.org/10.3109/01480545.2013.838776.

[11] N.J. Fox, G.W. Stachowiak, Vegetable oil-based lubricants—a review of oxidation, Tribol. Int. 40 (7) (2007) 1035–1046, https://doi.org/10.1016/j.triboint.2006.10.001.

[12] M.A. Fazal, F. Sundus, H.H. Masjuki, S. Rubaiee, M.M. Quazi, Tribological assessment of additive doped B30 biodiesel-diesel blend by using high frequency reciprocating rig test, Sustain Energy Technol Assess 48 (2021) 101577, https://doi.org/10.1016/j.seta.2021.101577.

[13] F.T. Hong, A. Schneider, S.M. Sarathy, Enhanced lubrication by core-shell TiO2 nanoparticles modified with gallic acid ester, Tribol. Int. 146 (2020) 106263, https://doi.org/10.1016/j.triboint.2020.106263.

[14] M. Fan, C. Zhang, P. Wen, W. Sun, R. Dong, D. Yang, W. Li, F. Zhou, W. Liu, High-performance lubricant base stocks from biorenewable gallic acid: systematic study on their physicochemical and tribological properties, Ind. Eng. Chem. Res. 56 (34) (2017) 9513–9523, https://doi.org/10.1021/acs.iecr.7b01452.
[15] V.R. Salinas Ruiz, T. Kuwahara, J. Galipaud, K. Masenelli-Varlot, M.B. Hassine, C. Héau, M. Stoll, L. Mayrhofer, G. Moras, J.M. Martin, M. Moseler, M.I. De Barros Bouchet, Interplay of mechanics and chemistry governs wear of diamond-like carbon coatings interacting with ZDDP-additivated lubricants, Nat. Commun. 12 (1) (2021) 1–15, https://doi.org/10.1038/s41467-021-24766-6.
[16] K.L. Johnson, Contact Mechanics, Cambridge University Press, 1985, https://doi.org/10.1017/CBO9781139171731.
[17] S. Loehlé, C. Matta, C. Minfray, T. Le Mogne, R. Iovine, Y. Obara, A. Miyamoto, J. M. Martin, Mixed lubrication of steel by C18 fatty acids revisited. Part II: in of some key parameters, Tribol. Int. 94 (2016) 207–216, https://doi.org/10.1016/j.triboint.2015.08.036.
[18] G. Kresse, J. Furthmü, Efficient iterative schemes for ab initio total-energy calculations using a plane-wave basis set, Phys. Rev. B 54 (1996) 11169, https://doi.org/10.1103/PhysRevB.54.11169.
[19] J.P. Perdew, K. Burke, M. Ernzerhof, Generalized gradient approximation made simple, Phys. Rev. Lett. 77 (1996) 3865, https://doi.org/10.1103/PhysRevLett.77.3865.
[20] S. Grimme, Semiempirical GGA-type density functional constructed with a long-range dispersion correction, J. Comput. Chem. 27 (15) (2006) 1787–1799, https://doi.org/10.1002/jcc.20495.
[21] T. Bučko, J. Hafner, S. Lebègue, J.G. Ángyán, Improved description of the structure of molecular and layered crystals: ab initio DFT calculations with van Der Waals corrections, J. Phys. Chem. A 114 (43) (2010) 11814–11824, https://doi.org/10.1021/jp106469x.
[22] H.T.T. Ta, M. Ferrario, S. Loehlé, M.C. Righi, Ab initio informed machine learning potential for tribochemistry and mechanochemistry: application for eco–friendly gallate lubricant additive, Computational Materials Today 1 (2024) 100005, https://doi.org/10.1016/j.commt.2024.100005.
[23] H. Wang, L. Zhang, J. Han, DeePMD-kit: a deep learning package for many-body potential energy representation and molecular dynamics, Comput. Phys. Commun. 228 (2018) 178–184, https://doi.org/10.17632/hvfh9yvncf.1.
[24] Y. Zhang, H. Wang, W. Chen, J. Zeng, L. Zhang, H. Wang, DP-GEN: A concurrent learning platform for the generation of reliable deep learning based potential energy models, Comput. Phys. Commun. 253 (2020) 107206, https://doi.org/10.17632/sxybkgc5xc.1.
[25] A. Pacini, M. Ferrario, S. Loehle, et al., Advancing tribological simulations of carbon-based lubricants with active learning and machine learning molecular dynamics, Eur. Phys. J. Plus 139 (2020) 549, https://doi.org/10.1140/epjp/s13360-024-05348-z.
[26] S. Plimpton, Fast parallel algorithms for short-range molecular dynamics, J. Comput. Phys. 117 (1995) 1, https://doi.org/10.1006/jcph.1995.1039.
[27] B. Gunawardana, P.J. Swedlund, N. Singhal, M.K. Nieuwoudt, Pentachlorophenol dechlorination with zero valent iron: a Raman and GCMS study of the complex role of surficial iron oxides, Environ. Sci. Pollut. Res. 25 (18) (2018) 17797–17806, https://doi.org/10.1134/1.1538292.
[28] A. Dychalska, P. Popielarski, W. Franków, K. Fabisiak, K. Paprocki, M. Szybowicz, Study of CVD diamond layers with amorphous carbon admixture by Raman scattering spectroscopy, Mater Sci Pol 33 (4) (2015) 799–805, https://doi.org/10.1515/msp2015-0067.
[29] R. Cabrera-Alonso, E. Guevara, M.G. Ramírez-Elías, B. Moncada, F.J. González, Detection of hydroquinone by Raman spectroscopy in patients with melasma before and after treatment, Skin Res. Technol. 25 (1) (2019) 20–24, https://doi.org/10.1111/srt.12589.
[30] S. Sirivisoot, B.S. Harrison, Magnetically stimulated ciprofloxacin release from polymeric microspheres entrapping iron oxide nanoparticles, Int. J. Nanomed. 10 (2015) 4447, https://doi.org/10.2147/IJN.S82830.
[31] Y. Long, J. Galipaud, V. Weihnacht, S. Makowski, J.M. Martin, M.I.D.B. Bouchet, Achieving superlubricity using selected tribo-pairs lubricated by castor oil and unsaturated fatty acids, Tribol. Int. 169 (2022) 107462, https://doi.org/10.1016/j.triboint.2022.107462.
[32] C. Gattinoni, J.P. Ewen, D. Dini, Adsorption of surfactants on α-Fe2O3(0001): a density functional theory study, J. Phys. Chem. C 122 (36) (2018) 20817–20826, https://doi.org/10.1021/acs.jpcc.8b05899.
[33] X. Yang, J. Dang, C. Zhang, J. Li, S. Niu, H. Gao, B. Liu, Z. Guo, H. Ma, Comparing the catalytic effect of metals for energetic materials: machine learning prediction of adsorption energies on metals, Langmuir 40 (1) (2024) 1087–1095, https://doi.org/10.1021/acs.langmuir.3c03348.
[34] M. Eder, K. Terakura, J. Hafner, Initial stages of oxidation of (100) and (110) surfaces of iron caused by water, Phys Rev B Condens Matter Mater Phys 64 (11) (2001), https://doi.org/10.1103/PhysRevB.64.115426.
[35] Y.K. Shin, H. Kwak, A.V. Vasenkov, D. Sengupta, A.C.T. Van Duin, Development of a ReaxFF reactive force field for Fe/Cr/O/S and application to oxidation of butane over a pyrite-covered Cr2O3 catalyst, ACS Catal. 5 (12) (2015) 7226–7236, https://doi.org/10.1021/acscatal.5b01766.
[36] C.A. Latorre, J.P. Ewen, C. Gattinoni, D. Dini, Simulating surfactant-iron oxide interfaces: from density functional theory to molecular dynamics, J. Phys. Chem. B 123 (31) (2019) 6870–6881, https://doi.org/10.1021/acs.jpcb.9b02925.
[37] J.P. Ewen, C. Gattinoni, N. Morgan, H.A. Spikes, D. Dini, Nonequilibrium molecular dynamics simulations of organic friction modifiers adsorbed on iron oxide surfaces, Langmuir 32 (18) (2016) 4450–4463, https://doi.org/10.1021/acs.langmuir.6b00586.
[38] P. Studt, Boundary lubrication: adsorption of oil additives on steel and ceramic surfaces and its influence on friction and wear, Tribol. Int. 22 (2) (1989) 111–119, https://doi.org/10.1016/0301-679X(89)90171-0.
[39] B.M. Fry, M.Y. Chui, G. Moody, J.S. Wong, Interactions between organic friction modifier additives, Tribol. Int. 151 (2020) 106438, https://doi.org/10.1016/j.triboint.2020.106438.
[40] B. Badhani, N. Sharma, R. Kakkar, Gallic acid: a versatile antioxidant with promising therapeutic and industrial applications, RCS Adv 5 (35) (2015) 27540–27557, https://doi.org/10.1039/C5RA01911G.
[41] G.C.H.H. Nijenbanning, C.H. Venner, H. Moes, Film thickness in elastohydrodynamically lubricated elliptic contacts, Wear 176 (2) (1994) 217–229, https://doi.org/10.1016/0043-1648(94)90150-3.
[42] H. Wang, Y. Liu, W. Liu, Y. Liu, K. Wang, J. Li, T. Ma, O.L. Eryilmaz, Y.J. Shi, A. Erdemir, J. Luo, Superlubricity of polyalkylene glycol aqueous solutions enabled by ultrathin layered double hydroxide nanosheets, ACS Appl. Mater. Interfaces 11 (22) (2019) 20249–20256, https://doi.org/10.1021/acsami.9b03014.
[43] P.T. Mikulski, J.A. Harrison, Packing-density effects on the friction of n-alkane monolayers, J. Am. Chem. Soc. 123 (28) (2001) 6873–6881, https://doi.org/10.1021/ja010189u.